Journal of Materials Chemistry A

ROYAL SOCIETY OF CHEMISTRY

PAPER

View Article Online
View Journal | View Issue

Cite this: J. Mater. Chem. A, 2025, 13, 37367

Immobilising molecular redox mediators for the oxygen evolution reaction using self-assembled monolayers

Samar Gharbi, [a] Isaac Alcón, [b] Jordi Ribas-Ariño, [b] Núria Crivillers, [a] Stefan T. Bromley *[bc] and Marta Mas-Torrent *[a]

The development of efficient and economical electrocatalysts for the oxygen evolution reaction (OER) that are stable and free of noble metals remains a significant scientific and technological challenge. The use of redox mediators (RMs) offers a promising approach to enhance the efficiency of electrocatalysts for a range of applications. However, the migration of the RM molecules between the electrodes, also known as shuttle effect, leads to undesirable redox side reactions and a reduction of the OER performance. Here, we introduce a novel approach to overcome this limitation by showing how covalently attaching RMs to the electrode surface through self-assembled monolayers (SAMs) is a promising route to immobilize them and prevent their diffusion into the electrolyte. For this purpose, we prepared different SAMs using two types of RMs based on tetrathiafulvalene (TTF) derivatives and using indium tin oxide (ITO) and fluorine doped tin oxide (FTO) as substrates. All electrodes showed efficient electrocatalytic activity under alkaline conditions. In this small proof-of-concept set of systems, we could achieve an OER performance with an overpotential of 400 mV at 0.25 mA cm^{-2} and a Tafel slope of 103 mV dec^{-1}. We rationalise these experimental findings with computational chemical modelling, which suggests that further improvements could be achieved through targeted chemical modifications to tune the highest occupied molecular orbital energy in these TTF-based RMs. Thus, this work demonstrates that covalent immobilization of RMs *via* SAMs offers a robust platform for the rational molecular engineering of electrocatalysts.

Received 25th June 2025
Accepted 27th September 2025

DOI: 10.1039/d5ta05164a

rsc.li/materials-a

1. Introduction

The world's energy needs are mainly fulfilled by burning fossil fuels, which are finite and depleting rapidly. This dependency is diminishing resources and harming the environment, which underlines the need to find sustainable energy solutions. Hydrogen is an alternative clean fuel which has enormous potential to be the cornerstone of sustainable energy production, storage and use.[1] The hydrogen economy has the potential to fundamentally revolutionize sectors such as shipping, industrial chemical production[2] and aviation,[3] through renewable-based energy production, efficient energy storage and sustainable energy distribution.[4]

Water electrocatalysis is the most environmentally friendly and efficient method for producing hydrogen[5] and a key process in energy storage systems such as solar fuel production,[6] supercapacitors[7] and metal–air batteries.[8] The oxidation of water, namely the oxygen evolution reaction (OER), is a critical step in water splitting. However, this process presents significant challenges due to its slow kinetics and high overpotential, which limit overall system efficiency. Commonly, Ru- and Ir-based electrocatalysts are deployed as for the OER. The scarcity and high cost of such materials is a critical issue and, thus, there is a huge interest in developing more affordable electrocatalysts.[9]

Redox mediators (RMs) that are soluble in the electrolyte media have recently attracted considerable attention as homogenous electrocatalysts for improving the OER. A variety of organic[10–12] and inorganic[13,14] RMs have been explored in the literature to accelerate OER kinetics and minimize overpotentials. For example, in lithium–oxygen ($Li–O_2$) batteries, RMs can facilitate the charging process using their intrinsic redox activity. This approach reduces the polarization effects, even in the presence of the discharge insulating medium, thus improving energy efficiency.[15,16] In this context, the electron donor molecule tetrathiafulvene (TTF) has been investigated as a highly efficient RM.[17] TTF can be easily and reversibly oxidised to its corresponding radical cation and dication species. These

[a]Institut de Ciència de Materials de Barcelona (ICMAB-CSIC), Campus de la UAB Bellaterra, 08193, Spain. E-mail: mmas@icmab.es
[b]Departament de Ciència de Materials i Química Física, Institut de Química Teòrica i Computatcional (IQTCUB), Universitat de Barcelona, c/Martí i Franquès 1-11, 08028 Barcelona, Spain. E-mail: s.bromley@ub.edu
[c]Institució catalana de Recerca i Estudis Avançats (ICREA), Passeig Lluís Companys 23, 08010 Barcelona, Spain

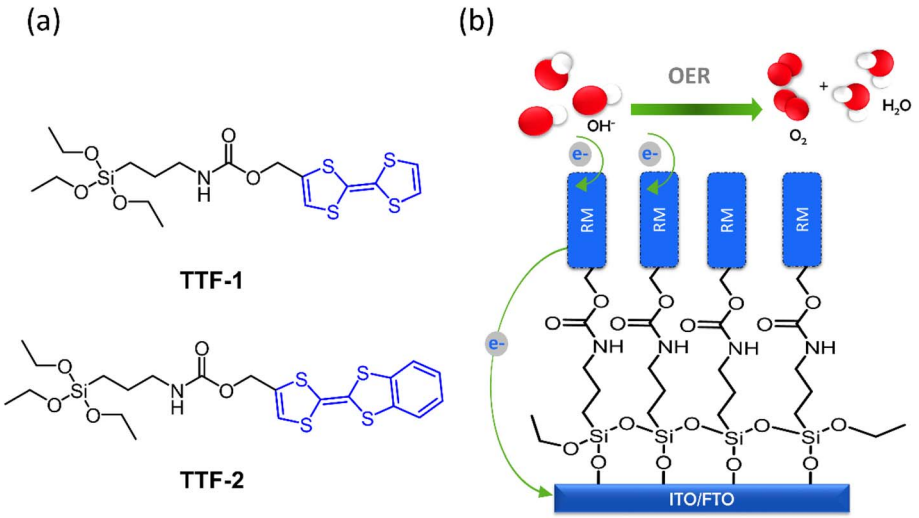

Scheme 1 (a) Chemical structures of our considered TTF derivatives. (b) Simplified illustration of the RM-SAMs (**TTF-1** and **TTF-2**) involved in the OER to promote water splitting to produce oxygen.

two oxidation states are stable as a result of a stepwise aromatization of the two dithiolylidene rings. Further, the extensive synthetic chemistry developed for TTFs allows for a systematic modification of their structural and electronic properties. As RM, TTF acts as an electron–hole transfer agent. During charging, TTF is oxidized to TTF^+ at the electrode surface. Subsequently, TTF^+ oxidizes solid Li_2O_2 products and then returns to the neutral initial state. As a result, TTF effectively decomposes Li_2O_2 at a lower charging potential.[18]

However, the migration of the highly mobile RM molecules between the electrodes may lead to undesirable redox side reactions. This so-called shuttle effect can lead to the unwanted consumption of the RM and can compromise the integrity of the electrolyte and/or electrode substrate, reducing the performance during sustained cycling.[19] Thus, a variety of strategies have been followed to suppress the shuttle effect. These include the use of electrolyte additives, electrode separators or electrode modifications.[20] The latter consists in restraining the RMs to be close to their partner electrode trying to avoid its diffusion towards the electrolyte, which is typically realized by preparing composite electrodes incorporating synthesized polymeric RMs.

The use of self-assembled monolayers (SAMs) of molecules chemically bonded on a substrate represents a powerful, inexpensive and versatile strategy for the modification of surfaces. SAMs are formed from the spontaneous organisation of molecules that have been designed with a suitable linker and a surface grafting group. SAMs have been exploited in many fields ranging through biosensing, molecular electronics, corrosion protection and surface wettability control, among many others.[21–23] Specifically, TTF-based SAMs have been reported for applications in ion sensors[24] and as robust electrochemical switches.[25]

Herein, we report the use of TTF-SAMs as surface-grafted RMs and demonstrate, for the first time, their efficiency as electrocatalysts for the OER, assisting the electron transfer between water and the electrodes to produce oxygen (Scheme 1). Two different molecular systems, **TTF-1** and **TTF-2** (Scheme 1), were designed to exhibit different electronic properties while both incorporating a terminal triethoxysilane group to enable covalent bonding with indium tin oxide (ITO) and fluorine-doped tin oxide (FTO) electrodes. All SAMs demonstrated electrocatalytic activity under alkaline conditions. However, **TTF-2**-SAMs exhibited superior efficiency and stability, which was attributed to the lower energy level of its highest occupied molecular orbital (HOMO). We support these experimental findings with density functional theory (DFT) calculations, which were also employed to suggest alternative TTFs with tuned electronic properties that could be exploited to further enhance the SAM-based electrocatalytic performance in the future.

2. Results and discussion

Two different RMs for OER have been designed, namely **TTF-1** and **TTF-2** (Scheme 1a), to be grafted on ITO and FTO substrates. The two electroactive molecules were synthesized according to methods described in the literature[26] (see Schemes S1, S2 and Fig. S1–S7 in the SI and Experimental section). The RM-SAMs were prepared by immersing the freshly cleaned substrates in a 1 mM solution of the corresponding RM in dry toluene under inert atmosphere and heating at 80 °C for the first 3 hours and then at room temperature for 24 hours. Following this procedure, we obtained four different RM-modified electrodes: **TTF-1**–ITO, **TTF-1**–FTO, **TTF-2**–ITO and **TTF-2**–FTO. It should be highlighted that supramolecular interactions between the surface-grafted molecules – specifically lateral π–π interactions between the planar TTF units and hydrogen bonding interactions between the amide groups – favor a uniform distribution of the electrocatalysts and improve the intramolecular charge transport.

The different SAMs were successfully characterized by X-ray photoelectron spectroscopy (XPS) (Table S1). In all the cases, the peaks found at ~285 eV and ~530 eV were assigned to oxygen-carbon bonds, while the peaks at ~164 eV were attributed to sulfur–carbon bonds and the ones at ~102 eV to silicon–oxygen bonds.[25] These findings confirm the RM bonding to the electrode surface.

The electrochemical behavior of the SAMs was investigated using cyclic voltammetry (CV) in dry acetonitrile (see Experimental section). These experiments were performed in a three-electrode electrochemical cell using the modified electrodes as working electrode, $Ag/AgNO_3$ as reference electrode and a platinum wire as counter electrode. The CV of **TTF-1** and **TTF-2** SAMs on each substrate are shown in Fig. 1a and b, respectively (see also Fig. S8). All the SAMs exhibit two reversible one-electron redox waves assigned to the formation of the radical-cation and dication species, as expected for TTF derivatives.[27,28] The asymmetric shape observed in the CVs is characteristic of dense TTF SAMs and has previously been ascribed to intermolecular electron interactions within the monolayer.[29–32]

As can be seen in Table 1, **TTF-2** shows higher redox potentials with respect to **TTF-1**. In particular, the first oxidation potential of the SAMs shifts from around 0.1–0.2 V in the case of **TTF-1** to approximately 0.4 V for the **TTF-2** derivative, while the second oxidation potential goes from 0.5 V to 0.8 V, respectively, for both types of electrodes. Further, from the first anodic peak integration, the molecular surface coverage (Γ) of the SAMs at 0.25 V s^{-1} was calculated (Table 1 and Experimental section). It is noticed that both molecules form denser SAMs on the ITO substrates. In addition, **TTF-2** leads to higher surface coverage SAMs compared to **TTF-1**. This can be ascribed to the greater ability of **TTF-2** to form denser SAMs thanks to extended lateral π–π intermolecular interactions and to the smoother ITO surface.[33] Atomic Force Microscopy (AFM) topography images of the ITO and FTO electrode (Fig. S9), revealed a Root Mean Square (RMS) roughness of 6 nm and 20 nm, respectively. The stability of the SAMs was explored by applying 40 consecutive CV cycles. Analyzing the current intensity over time, a negligible current loss in the SAMs on ITO during redox cycles was observed (Fig. S10). On the other hand, with the FTO electrodes a current loss was observed in the first switching cycles until it became stabilized. This may originate from the presence of physisorbed TTF molecules on the FTO surface.

The first oxidation potentials of the SAMs were also estimated by performing the CV in aqueous media (see Fig. S11). **TTF-1** exhibits a first oxidation potential around 0.8–0.9 V *vs.* the reversible hydrogen electrode (RHE), while **TTF-2** is oxidized

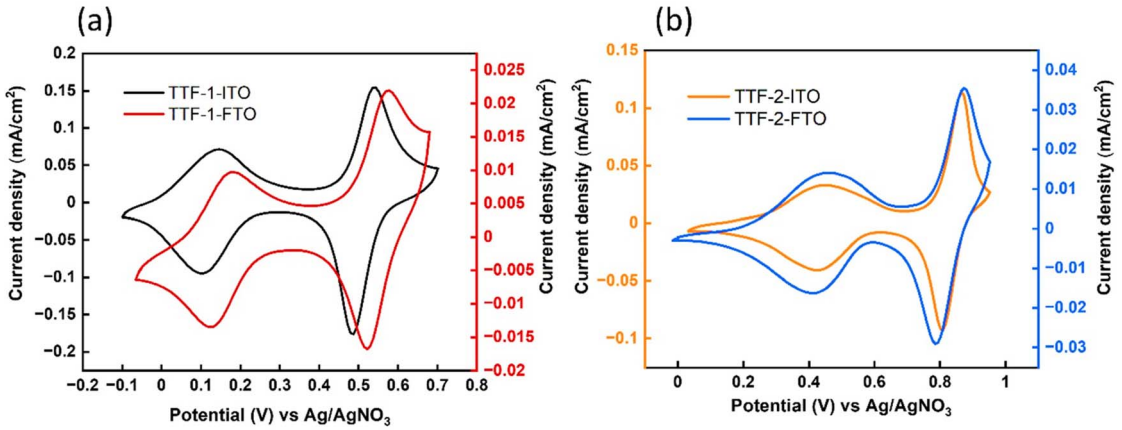

Fig. 1 Cyclic voltammetry of (a) **TTF-1** on ITO/FTO and (b) **TTF-2** on ITO/FTO, in a 0.1 M $LiClO_4$ solution in acetonitrile (scan rate = 0.25 V s^{-1}).

Table 1 Electrochemical data for **TTF-1**/**TTF-2** SAMs on ITO and FTO substrates estimated by CV (standard redox potentials ($E_1^{1/2}$ and $E_2^{1/2}$), surface coverage (Γ) and estimated HOMO level), OER overpotential of the SAMs and the bare electrodes at 0.25 mA cm^{-2}, and theoretical HOMO level estimated by DFT

Electrode	RM	$E_1^{1/2}/E_2^{1/2}$ (V *vs.* $Ag/AgNO_3$) in CH_3CN[a]	$E_2^{1/2}$ (V *vs.* RHE) in H_2O[b]	Γ[a] (mol cm^{-2})	Overpotential[c] (mV)	Experimental HOMO[a] (eV)	Theoretical HOMO (eV)
FTO	**TTF-1**	0.18/0.56	0.87	5.27×10^{-11}	420 ± 26	−4.60 ± 0.01	−4.76
ITO	**TTF-1**	0.12/051	0.82	3.22×10^{-10}	490 ± 15	−4.56 ± 0.01	
FTO	**TTF-2**	0.43/0.84	1.10	2.77×10^{-10}	400 ± 25	−4.84 ± 0.02	−4.90
ITO	**TTF-2**	0.42/083	1.11	5.56×10^{-10}	430 ± 17	−4.85 ± 0.01	
FTO	None	—	—	—	560	—	—
ITO	None	—	—	—	530	—	—

[a] Electrolyte media: 0.1 M $LiClO_4$ in CH_3CN. [b] Electrolyte media: 0.1 M $LiClO_4$ in water. [c] Electrolyte media: 1 M KOH in water (pH = 14).

at 1.1 V *vs.* RHE (Table 1). These values are below the standard oxidation potential for water splitting (1.23 *vs.* RHE).

The OER electrocatalytic activity of the RM SAMs was studied using a standard three-electrode electrochemical cell in a 1 M KOH aqueous solution (pH = 14) using an Ag/AgCl electrode as reference. The linear sweep voltammograms (LSV) of the RM-SAMs on ITO are shown in Fig. 2a together with the curve corresponding to the blank non-modified ITO electrode, while the ones related to the FTO electrodes can be found in Fig. 2b. The horizontal grey dashed line indicates the potential associated to the RHE. All the RM modified electrodes exhibit an OER electrocatalytic effect, as demonstrated by the increase in the measured current and shifting of the onset voltage, to lower potentials, with respect to the blank electrodes. In alkaline OER conditions, the positively charged TTFs can adsorb OH^- through electrostatic forces, consequently promoting the electron transfer between the catalyst surface and oxygen species, resulting in the observed improvement of the OER activity.[34,35]

The overpotential (η) was calculated at a standardized current density of 0.25 mA cm^{-2} to ensure consistency in the comparison (Table 1). The RM **TTF-2** shows an enhanced electrocatalytic activity on both ITO/FTO electrodes compared to **TTF-1**. Notably, **TTF-2**–FTO reveals the lowest overpotential of 400 mV and the highest catalytic current density over a wide potential range compared to the other cases. With regards to the electrode type, the OER electrocatalytic efficiency is improved for both TTF derivatives with the FTO electrode. It has already been reported that FTO exhibits a higher chemical stability than ITO in electrochemical operation, reducing its surface degradation.[36]

Electrochemical impedance spectroscopy (EIS) was performed on the TTF-SAMs at a potential of 1.62 V *versus* RHE (Fig. S12). In the Nyquist plots, **TTF-2**–FTO shows the smallest semicircle corresponding to the lowest charge transfer resistance and indicating a higher charge transfer rate for OER.

To evaluate the stability of the modified electrodes during the OER process, a chronopotentiometric experiment was performed holding a constant current of 1 mA at the working electrode. It was found that the initial activity of **TTF-2**–ITO and **TTF-2**–FTO electrodes remained unchanged after 14 000 seconds (*i.e.*, almost 4 hours) of continuous operation (Fig. 2c), while **TTF-1**–FTO and **TTF-1**–ITO showed an unstable potential under the same conditions (Fig. S13). During the chronopotentiometry test the formation of oxygen bubbles was clearly visible on the surfaces of the electrodes modified with **TTF-2**, indicating the production of oxygen gas resulting from the OER (Fig. S14). The higher stability of **TTF-2** during the OER could be again accounted to the enhanced π–π intermolecular interactions present between the TTF units. It was estimated by CV that the molecular surface coverage of **TTF-2**–ITO after the

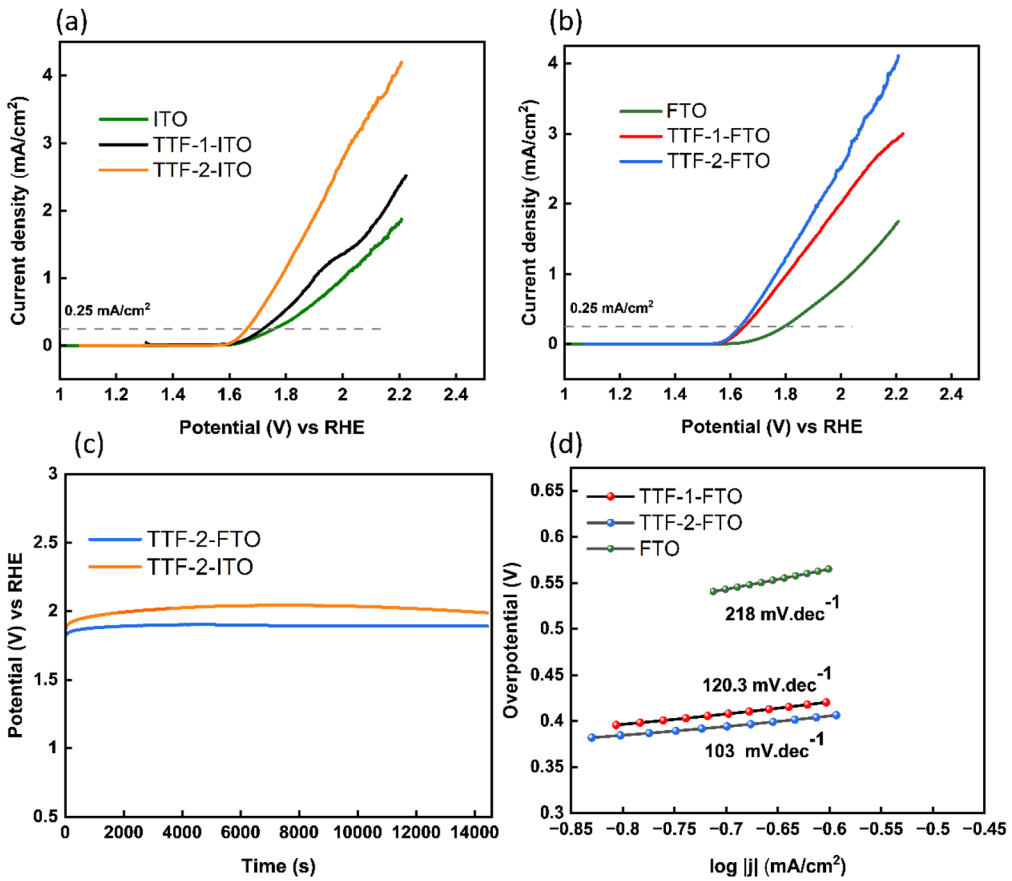

Fig. 2 LSV of SAMs on (a) ITO and (b) FTO. (c) Chronopotentiometry curves of **TTF-2** SAMs. (d) Tafel plots for FTO, **TTF-1**–FTO and **TTF-2**–FTO. All measurements were performed in 1.0 M KOH aqueous solution as electrolyte (pH = 14).

OER experiment was a 92% of the initial value, pointing to a low molecular desorption.

To verify that the observed OER electrocatalytic effect is due to the electroactive character of the RM and not due to the surface modification of the electrodes, we also modified the electrodes with the non-electroactive molecule propyltriethoxysilane (PTES), which was studied under the same conditions. As can be seen in Fig. S15, PTES shows the highest overpotential (530 mV for PTES–ITO and 670 mV for PTES–FTO), which is even higher than those of the bare electrodes. This can be explained by the steric blocking of the electrodes that leads to a reduction of their ability to transfer electrons to the aqueous solution, thus diminishing their overall electrocatalytic activity. This cross-check experiment highlights the key role of the RMs studied herein to improve the electrocatalytic performance.

A Tafel analysis was carried out to study the OER kinetics, which consists in representing the overpotential as a function of current density (j) on a logarithmic scale. The Tafel slope is a kinetic parameter that provides insight about the electron transfer process. The lower the Tafel slope, the faster the

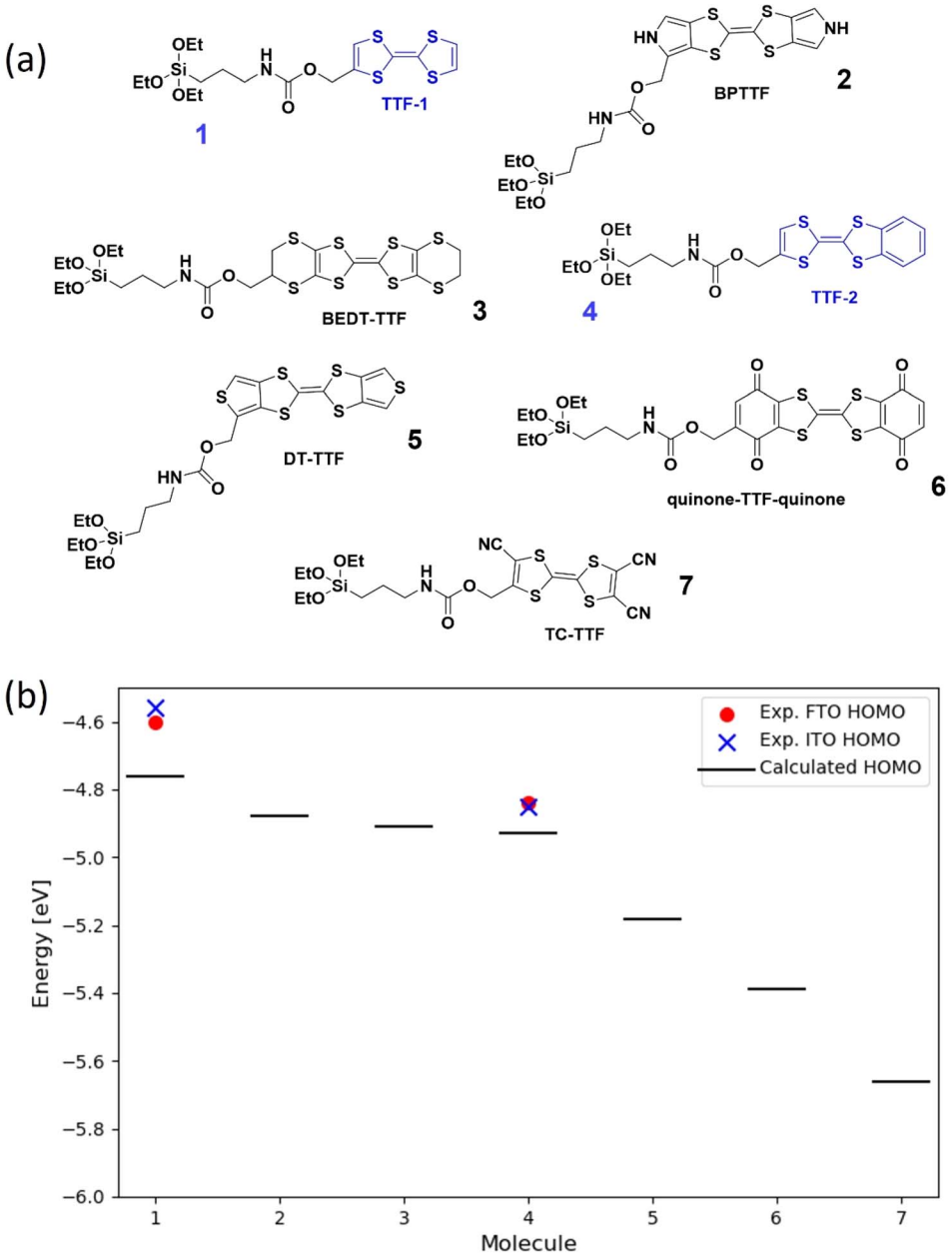

Fig. 3 (a) Chemical structures of different TTF derivatives. The experimentally synthesized derivatives are highlighted in blue (**TTF-1** and **TTF-2**). Molecules are sorted by decreasing calculated HOMO values. (b) Corresponding HOMO energies calculated with implicit solvation to account for the acetonitrile medium (see Experimental section for details). The experimentally determined HOMO values (*via* CV measurements) are included both for ITO-supported SAMs (blue crosses) and FTO-supported SAMs (red spheres) for **TTF-1** (# 1 in the series) and **TTF-2** (# 4 in the series).

electron transfer kinetics.[37] Fig. 2d shows the Tafel curves of FTO and the RM-FTO electrodes, while the corresponding plot for the ITO electrodes is shown in Fig. S16. It is observed that the bare FTO electrode has a Tafel slope of 218 mV dec^{-1}. However, this value is significantly decreased to 120 mV dec^{-1} and 103 mV dec^{-1} upon surface modification with RMs **TTF-1** and **TTF-2**, respectively, highlighting a faster charge-transfer process for both of them. A similar behavior was observed for ITO electrodes functionalized with **TTF-2** (see Fig. S16).

The OER activity of catalysts varies considerably depending on their composition, structural class and experimental conditions. Hence, performance comparisons should be taken with caution. However, in order to contextualize our results, in Table S2 the reported overpotentials of different types of non-noble metal-based catalysts in alkali media have been collected. Considering this, our SAM-based TTF derivatives show a competitive performance, emphasizing the growing potential of molecularly engineered organic systems in OER electrocatalysis.

Considering all the above, we can state that both RM-SAMs exhibit an efficient electrocatalytic performance, although **TTF-2** shows a higher efficiency than **TTF-1**. This can be rationalized considering the different electronic properties of the two molecules. The role of the RM in the OER is to assist the transfer of electrons from the water molecules to the electrodes, promoting their dissociation. This process is required for the subsequent formation of oxygen–oxygen bonds in the OER.[38,39] Therefore, the energy level of the HOMO of the electron-donating RM is particularly critical. The HOMO levels of the **TTF-1** and **TTF-2** SAMs were experimentally estimated from the first oxidation potential extracted from the CV data (Table 1), as described in the Experimental section. It can be seen that **TTF-2** SAMs have a HOMO level around 0.25–0.30 eV lower than that of the **TTF-1** SAMs, which results in a higher electrocatalytic efficiency (see discussion below).

In line with this experimental procedure, we calculated the first oxidation potential of **TTF-1** and **TTF-2** using DFT calculations (see Table 1). Here, the influence of the acetonitrile solvent used in the CV experiments is also taken into account. As the calculated energies are automatically referenced to the vacuum level, the negative of the calculated first oxidation potential can be directly compared with the experimentally estimated HOMO energy values. We can see in Table 1 that the theoretically determined HOMO values are in good agreement with the experimental values, with the difference being 0.2 eV for **TTF-1** and 0.1 eV for **TTF-2**. We note that the calculations were performed on the solvated molecule only and thus do not take into account possible substrate effects.

Based on the good agreement between the theoretically and experimentally determined HOMO values, we have computationally screened a set of chemically viable TTF derivatives (Fig. 3).[40,41] Here, the experimentally synthesized **TTF-1** and **TTF-2** appear in positions 1 and 4 in Fig. 3b, respectively, and the experimentally obtained HOMO levels for these systems are highlighted. Generally, we find that varying the chemical structure of the TTF allows for a significant tuning of the resulting HOMO energy. Specifically, in our set of derivatives, we find that the HOMO value may be varied by nearly ~1 eV *via* chemical design. We note that attaching functional groups with a high electronegative character, such as in derivatives **6** and **7**, appears to be the most efficient manner to lower the HOMO level. We also notice that the computed HOMO levels are not significantly altered by the tether chain for the selected TTF derivatives (Fig. S17). This highlights that the HOMO values are mostly determined by the TTF core and its specific chemical functionalization. As previously mentioned, the thermodynamic standard redox potential of the OER is 1.23 V *vs.* RHE. However, due to kinetic barriers, an additional overpotential is typically required to drive the reaction. As a result, the OER commonly occurs within the potential range of 1.4 to 1.8 V *vs.* RHE.[42,43] For a RM to be more efficient, its oxidation potential should be aligned or slightly higher than the OER potential.[44–46] Considering that the redox potential of **TTF-2** is around 1.1 V *vs.* RHE, we can anticipate that our theoretically proposed TTF derivatives **6** and **7** might exhibit an improved OER electrocatalytic performance, if experimentally realized. This is due to the fact that these derivatives reveal a lower-lying HOMO level that would lead to higher oxidation redox potentials in the range 1.6–1.8 V *vs.* RHE.

3. Conclusions

In summary, the electrocatalytic behavior of two RM SAMs covalently immobilised on electrode surfaces towards the OER was investigated. In particular, self-assembled monolayers of two TTF derivatives, **TTF-1** and **TTF-2**, differing in their oxidation potentials were prepared on ITO and FTO substrates. Both systems exhibited an electrocatalytic effect under alkaline conditions, although **TTF-2** SAM showed a superior OER performance with a lower overpotential of 400 mV at 0.25 mA cm^{-2}, along with an improved stability under continuous operation. This improved performance was attributed to the lower-lying HOMO level of **TTF-2**. Theoretical calculations further predicted that the chemical substitution of the TTF core could significantly lower the HOMO energy, potentially leading to an additional enhancement of the OER electrocatalytic efficiency.

Overall, this works demonstrates that covalent attachment of RMs to electrode surfaces represents a promising route to mitigate the shuttle effect and reduce OER overpotentials. This concept can be further extended to other redox-active molecules and to a wide range of important electrochemical reactions. Our work highlights that targeted molecular design can be employed to develop tunable molecular RMs tailored to specific reaction requirements. Finally, it should be emphasized that the RMs reported here are not derived from critical or costly materials, and that the formation of SAMs can be achieved through simple, low-cost, and inherently scalable processes highlighting the strong potential of this strategy for sustainable electrocatalysis. Future work will be devoted to gaining insights into the parameters affecting the electrocatalytic efficiency (*i.e.*, surface density, SAM thickness, *etc.*) as well as finding strategies for improving the electrochemical stability of the systems under harsh media.

4. Experimental section

Materials and methods

All reagents required for the synthesis of **TTF-1** and **TTF-2**, as well as the reagents for the electrochemical study, were purchased from Sigma-Aldrich and used as received. Solvents were purchased from Thermo Fisher Scientific and used without further purification. ^{1}HNMR and ^{13}C NMR spectra were recorded using a Bruker Advance 300 spectrometer. Fourier transform infrared (FT-IR) spectra were recorded using a PerkinElmer RX-1 instrument with a resolution of 1.0 ± 0.1 cm^{-1}. Commercial substrates of ITO (7 × 50 × 0.5 mm, R_s = 8–12 Ω) and FTO (7 × 35 × 0.9 mm, $R_s \leq 14$ Ω) on unpolished float glass were purchased from Delta Technologies. X-ray photoelectron spectroscopic measurements were performed using a Phoibos 150 analyzer under ultra-high vacuum conditions with a monochromatic aluminium K α X-ray source. Atomic force microscopy (AFM) was performed using a Keysight 5500 system equipped with a closed-loop scanner (90 × 90 μm X/Y, 15 μm Z), three lock-in amplifiers with external signal access. The Root Mean Square (RMS) roughness was determined using the Gwyddion software.

MALDI-TOF analysis was performed using a Bruker MicroFLE mass spectrometer, with the sample prepared using Dithranol (DIT) as the matrix, and spectra were recorded in positive ion mode.

Synthesis of TTF–CH_2–OH (2)

In a two-necked flask, $NaBH_4$ (73.83 mg, 0.51 mmol) was added to a commercial solution of 2-formyltetrathiafulvalene (**1**) (100 mg, 0.43 mmol) in 4.5 mL of MeOH. The solution was stirred for 30 minutes under an inert atmosphere. Then CH_2Cl_2 was added and the mixture was washed first with brine and then with water. The separated organic phase was dried with $MgSO_4$ and the solvent was evaporated. A yellow solid was obtained, which was purified by flash chromatography (eluent CH_2Cl_2). The compound TTF–CH_2–OH was obtained with a 50% yield (Scheme S1). The molecular structure of TTF–CH_2–OH was confirmed by ^{1}H NMR and FT-IR (Fig. S1 and S2).[47]

Synthesis of TTF-1. In an anhydrous system, a solution of TTF–CH_2–OH (**2**) (100 mg; 0.42 mmol) in dry THF (10 mL) was poured into a round-bottomed three-necked flask, triethylamine (86 μL; 0.85 mmol) was added under stirring for 15 min, and then 3-(isocyanotopropyl)triethoxysilane (ICTES) was added (116 μL; 0.47 mmol), the mixture was refluxed overnight. The solvent was evaporated at reduced pressure, yielding a yellow oil. The crude product was purified by column chromatography (ethyl acetate/dichloromethane 1 : 4). The **TTF-1** was obtained as a yellow product with a yield of 38% (Scheme S1). The molecular structure was confirmed by ^{1}H NMR, ^{13}C NMR and FT-IR as well as by MALDI-TOF (Fig. S3–S6).

Synthesis of TTF-2. The RM **TTF-2** was synthesized according to the same synthesis route detailed in our previous work (Scheme S2) and characterized by ^{1}HNMR (Fig. S7).[25]

Preparation of SAMs based on TTF derivatives

The FTO/ITO substrates were first cleaned in ultrasonic baths using a series of solvents with increasing polarity (dichloromethane, acetone and then ethanol) for 10 minutes each. The substrates were washed with pure ethanol and dried under a stream of nitrogen. Subsequently, the substrates were treated in an oxidizing bath of $NH_4OH : H_2O_2 : H2O$ (1 : 1 : 5) for 30 minutes to obtain a hydrophilic surface and then washed with distilled Millipore water, rinsed with ethanol and dried under a nitrogen flow. The freshly cleaned FTO/ITO substrates were immersed in a 1 mM solution of the corresponding RM (*i.e.*, **TTF-1** or **TTF-2**) in freshly distilled toluene in a vessel under argon atmosphere. They were heated at 80 °C for 3 hours and then stored at room temperature for 24 hours. Afterwards, the substrates were rinsed several times with toluene and dried under a stream of nitrogen.

Electrochemical measurements

All the electrochemical measurements were carried out using an Autolab PGSTAT101 using NOVA Advanced Electrochemical Software. The experiments were performed under inert conditions. Cyclic voltammograms were acquired at a scan rate of 0.25 V s^{-1}, using a 0.1 M of lithium perchlorate ($LiClO_4$) solution in dry acetonitrile, both the TTF-SAMs and the corresponding molecular redox mediators (**TTF-1** and **TTF-2**) in dilute dichloromethane solution (Fig. S8) were studied with the same setup, using $Ag/AgNO_3$ as the reference electrode, a platinum wire as the counter electrode, and the SAM/electrode or bare electrode as the working electrode.

The surface coverage (Γ) in mol cm^{-2} of the TTF redox-active SAMs was calculated using the following equation:

$$\Gamma = \frac{Q}{nFA}$$

where Q is the transferred charge during the oxidation of TTF to its radical cation form, n is the number of electrons involved in the redox reaction, F is Faraday's constant, and A is the electrode surface immersed in the electrolyte.

CV measurements were also performed in a 0.1 M solution of $LiClO_4$ in water using an Ag/AgCl reference electrode.

Oxygen evolution reaction (OER) performance

The OER was tested in a standard three-electrode electrochemical cell system at room temperature. The catalytic activity towards OER was measured in 1 M KOH (pH = 14) in MilliQ water by linear sweep voltammetry (LSV) at a scan rate of 5 mV s^{-1} using the different SAMs as working electrodes, platinum wire as counter electrode and the Ag/AgCl electrode as a reference electrode.

Electrochemical impedance spectroscopy (EIS) analysis was performed with a frequency ranging from 200 kHz to 5 mHz at a potential of 1.62 V *vs.* RHE and 0.01 V amplitude. Before starting the measurement, the electrolyte was degassed with argon for 10 minutes. The measured potentials with respect to Ag/AgCl reference electrode ($E_{Ag/AgCl}$) were converted with respect to RHE using the Nernst equation.[48]

$$E_{(\mathrm{RHE})} = E_{\mathrm{Ag/AgCl}} + 0.059 \times \mathrm{pH} + 0.197$$

The overpotentials (η) at 0.25 mA cm^{-2} were calculated using the following equation

$$\eta = E_{(\mathrm{RHE})} - 1.23\ \mathrm{V}$$

the Tafel slopes were calculated using the LSV curves with the Tafel equation

$$\eta = a + b \log j$$

where η represents the overpotential, j is the current density, a is a constant and b is the Tafel slope.[49,50]

The energy level of HOMO (E_{HOMO}) of the TTF derivatives in the SAMs was estimated from redox potentials determined by CV *versus* the ferrocene/ferrocenium redox couple (Fc/Fc^+):

$$E_{\mathrm{HOMO}} = E_{\mathrm{ox}}{}^{1/2} - 4.8\ \mathrm{eV}$$

where $E_{ox}{}^{1/2}$ is the half-wave oxidation potential of the TTF-SAMs and 4.8 eV is the energy level of the Fc/Fc^+ redox couple in vacuum.[51]

Stability tests

Chronopotentiometry was performed at 1 mA for 14 000 seconds to evaluate the stability of the SAMs through the OER experiments.

DFT calculations

The chemical structures of **TTF-1**, **TTF-2** and a selection of other TTFs (both with and without a tethering group) were computed using DFT calculations employing the PBE0 (ref. 52) hybrid functional and a def2TZVP basis set as implemented in the Gaussian16 code.[53] The HOMO levels of these systems were obtained by taking the negative of the calculated vertical first oxidation potential. These were computed as the energy difference between the neutral and cationic systems using the optimized geometry of the neutral system throughout. All molecules were optimized with implicit solvation using the polarizable continuum model,[54] choosing acetonitrile as solvent (as in the CV characterization).

Conflicts of interest

There are no conflicts to declare.

Data availability

The data is available upon request to the authors.

Supplementary information is available. See DOI: https://doi.org/10.1039/d5ta05164a.

Acknowledgements

This work was funded by MCIN/AEI/10.13039/501100011033/ERDF, UE with projects SENSATION PID2022-141393OB-I00, TED2021-132550B-C22, TED2021-132550B-C21 and PID2021-127957NB-I00 and through the "Severo Ochoa" Programme for Centers of Excellence in R&D (CEX2023-001263-S) and María de Maeztu program for Spanish Structures of Excellence (CEX2021-001202-M). The authors also acknowledge funds from Generalitat de Catalunya with projects 2021-SGR-00443, 2021-SGR-00354 and HYDROCAT 2023 CLIMA 00064.

References

1 M. G. Rasul, M. A. Hazrat, M. A. Sattar, M. I. Jahirul and M. J. Shearer, *Energy Convers. Manage.*, 2022, **272**, 116326.
2 N. Rambhujun, M. S. Salman, T. Wang, C. Pratthana, P. Sapkota, M. Costalin, *et al.*, *MRS Energy Sustain.*, 2020, **7**, E33.
3 T. Yusaf, A. S. F. Mahamude, K. Kadirgama, D. Ramasamy, K. Farhana, H. A. Dhahad and A. R. A. Talib, *Int. J. Hydrogen Energy*, 2024, **52**, 1026–1045.
4 S. Sharma and S. K. Ghoshal, *Renewable Sustainable Energy Rev.*, 2015, **43**, 1151–1158.
5 B. Ghorbani, S. Zendehboudi, Y. Zhang, H. Zarrin and I. Chatzis, *Energy Convers. Manage.*, 2023, **297**, 117599.
6 A. Berrada and M. A. Laasmi, *J. Energy Storage*, 2021, **44**, 103448.
7 J. Zhang, J. Zheng and W. Yang, *Chem. Eng. J.*, 2021, **403**, 126368.
8 Y. Chen, J. Xu, P. He, Y. Qiao, S. Guo, H. Yang and H. Zhou, *Sci. Bull.*, 2022, **67**, 2449–2486.
9 S. Sanati, R. S. Varma, M. Liu and R. Abazari, *Energy Environ. Sci.*, 2025, **18**, 7733–7755.
10 B. J. Bergner, A. Schürmann, K. Peppler, A. Garsuch and J. Janek, *J. Am. Chem. Soc.*, 2014, **136**, 15054–15064.
11 H. D. Lim, B. Lee, Y. Zheng, J. Hong, J. Kim, H. Gwon, *et al.*, *Nat. Energy*, 2016, **1**, 16066.
12 D. Kundu, R. Black, B. Adams and L. F. Nazar, *ACS Cent. Sci.*, 2015, **1**, 510–515.
13 H. D. Lim, H. Song, J. Kim, H. Gwon, Y. Bae, K. Y. Park, *et al.*, *Angew. Chem.*, 2014, **126**, 4007–4012.
14 H. Zhong, J. Wang, Y. Wang, P. He and H. Zhou, *Energy Fuels*, 2021, **35**, 19302–19319.
15 I. Landa-Medrano, I. Lozano, N. Ortiz-Vitoriano, I. Ruiz de Larramendi and T. Rojo, *J. Mater. Chem. A*, 2019, **7**, 8746–8765.
16 X. Shen, S. Zhang, Y. Wu and Y. Chen, *ChemSusChem*, 2019, **12**, 104–115.
17 Y. Chen, S. A. Freunberger, Z. Peng, O. Fontaine and P. G. Bruce, *Nat. Chem.*, 2013, **5**, 489–494.
18 Y. Dou, Z. Xie, Y. Wei, Z. Peng and Z. Zhou, *Natl. Sci. Rev.*, 2022, **9**, nwac040.
19 Y. Li, W. Yang, W. Yang, Y. Huang, G. Wang, C. Xu, *et al.*, *J. Energy Chem.*, 2021, **60**, 233–240.
20 X. Wu, W. Yu, K. Wen, H. Wang, X. Wang, C. W. Nan and L. Li, *J. Energy Chem.*, 2021, **60**, 135–149.
21 M. Mas-Torrent, C. Rovira and J. Veciana, *Adv. Mater.*, 2013, **25**, 462–468.
22 M. Singh, N. Kaur and E. Comini, *J. Mater. Chem. C*, 2020, **8**, 3938–3955.

23 L. Hao, X. Fu, T. Li, N. Zhao, X. Shi, F. Cui, *et al.*, *Colloids Surf., B*, 2016, **148**, 549–556.
24 D. Canevet, M. Sallé, G. Zhang, D. Zhang and D. Zhu, *Chem. Commun.*, 2009, 2245–2269.
25 M. A. Herranz, B. Colonna and L. Echegoyen, *Proc. Natl. Acad. Sci. U. S. A.*, 2002, **99**, 5040–5047.
26 C. Simao, M. Mas-Torrent, J. Casado-Montenegro, F. Otón, J. Veciana and C. Rovira, *J. Am. Chem. Soc.*, 2011, **133**, 13256–13259.
27 J. Jalkh, Y. R. Leroux, A. Vacher, D. Lorcy, P. Hapiot and C. Lagrost, *J. Phys. Chem. C*, 2016, **120**, 28021–28030.
28 E. Marchante, M. S. Maglione, N. Crivillers, C. Rovira and M. Mas-Torrent, *RSC Adv.*, 2017, **7**, 5636–5641.
29 Y. Yokota, A. Miyazaki, K. I. Fukui, T. Enoki, K. Tamada and M. Hara, *J. Phys. Chem. B*, 2006, **110**, 20401–20408.
30 M. A. Herranz, L. Yu, N. Martin and L. Echegoyen, *J. Org. Chem.*, 2003, **68**, 8379–8385.
31 W. F. Paxton, S. L. Kleinman, A. N. Basuray, J. F. Stoddart and R. P. Van Duyne, *J. Phys. Chem. Lett.*, 2011, **2**, 1145–1149.
32 J. Casado-Montenegro, M. Mas-Torrent, F. Otón, N. Crivillers, J. Veciana and C. Rovira, *Chem. Commun.*, 2013, **49**, 8084–8086.
33 F. Schreiber, *Prog. Surf. Sci.*, 2000, **65**, 151–257.
34 J. Suntivich, K. J. May, H. A. Gasteiger, J. B. Goodenough and Y. Shao-Horn, *Science*, 2011, **334**, 1383–1385.
35 X. Xie, L. Du, L. Yan, S. Park, Y. Qiu, J. Sokolowski and Y. Shao, *Adv. Funct. Mater.*, 2022, **32**, 2110036.
36 A. Korjenic and K. S. Raja, *J. Electrochem. Soc.*, 2019, **166**, C169–C184.
37 A. Trabolsi, G. Das, S. S. Roy, F. A. Ibrahim, A. Merhi, H. N. Dirawi, *et al.*, *Angew. Chem., Int. Ed.*, 2024, e202419836.
38 C. Yang, Z. D. Yang, H. Dong, N. Sun, Y. Lu, F. M. Zhang and G. Zhang, *ACS Energy Lett.*, 2019, **4**, 2251–2258.
39 Z. M. Chan, D. A. Kitchaev, J. N. Weker, C. Schnedermann, K. Lim, G. Ceder, *et al.*, *Proc. Natl. Acad. Sci. U. S. A.*, 2018, **115**, E5261–E5268.
40 M. Mas-Torrent and C. Rovira, *J. Mater. Chem.*, 2006, **16**, 433–436.
41 D. Canevet, M. Sallé, G. Zhang, D. Zhang and D. Zhu, *Chem. Commun.*, 2009, 2245–2269.
42 X. Gao, X. Bai, P. Wang, Y. Jiao, K. Davey, Y. Zheng and S. Z. Qiao, *Nat. Commun.*, 2023, **14**, 5842.
43 A. Raveendran, M. Chandran and R. Dhanusuraman, *RSC Adv.*, 2023, **13**, 3843–3876.
44 S. Huang and Q. Wang, *Acc. Mater. Res.*, 2023, **4**, 693–703.
45 L. Wu, A. Nayak, J. Shao and T. J. Meyer, *Proc. Natl. Acad. Sci. U. S. A.*, 2019, **116**, 11153–11158.
46 H. D. Lim, B. Lee, Y. Zheng, J. Hong, J. Kim, H. Gwon, *et al.*, *Nat. Energy*, 2016, **1**, 16066.
47 J. Sinha, S. J. Lee, H. Kong, T. W. Swift and H. E. Katz, *Macromolecules*, 2013, **46**, 708–717.
48 A. G. Rajan and E. A. Carter, *Energy Environ. Sci.*, 2020, **13**, 4962–4976.
49 A. Kapałka, G. Fóti and C. Comninellis, *Electrochem. Commun.*, 2008, **10**, 607–610.
50 F. T. Tsai, Y. T. Deng, C. W. Pao, J. L. Chen, J. F. Lee, K. T. Lai and W. F. Liaw, *J. Mater. Chem. A*, 2020, **8**, 9939–9950.
51 Y. Geng, R. Pfattner, A. Campos, W. Wang, O. Jeannin, J. Hauser, *et al.*, *Chem.–Eur. J.*, 2014, **20**, 16672–16679.
52 C. Adamo and V. Barone, *J. Chem. Phys.*, 1999, **110**, 6158–6170.
53 M. J. Frisch, G. W. Trucks, H. B. Schlegel, G. E. Scuseria, M. A. Robb, J. R. Cheeseman *et al.*, *Gaussian 16, Revision A.03*, Gaussian, Inc., Wallingford CT, 2016.
54 J. Tomasi, B. Mennucci and R. Cammi, *Chem. Rev.*, 2005, **105**, 2999–3094.